NANO LETTERS

pubs.acs.org/NanoLett

Efficient Coupling between Dielectric-Loaded Plasmonic and Silicon Photonic Waveguides

Ryan M. Briggs,*,† Jonathan Grandidier,† Stanley P. Burgos,† Eyal Feigenbaum,† and Harry A. Atwater†,‡

†Thomas J. Watson Laboratories of Applied Physics and ‡Kavli Nanoscience Institute, California Institute of Technology, Pasadena, California 91125, United States

ABSTRACT The realization of practical on-chip plasmonic devices will require efficient coupling of light into and out of surface plasmon waveguides over short length scales. In this letter, we report on low insertion loss for polymer-on-gold dielectric-loaded plasmonic waveguides end-coupled to silicon-on-insulator waveguides with a coupling efficiency of 79 ± 2% per transition at telecommunication wavelengths. Propagation loss is determined independently of insertion loss by measuring the transmission through plasmonic waveguides of varying length, and we find a characteristic surface-plasmon propagation length of 51 ± 4 μm at a free-space wavelength of $\lambda = 1550$ nm. We also demonstrate efficient coupling to whispering-gallery modes in plasmonic ring resonators with an average bending-loss-limited quality factor of 180 ± 8.

KEYWORDS Surface plasmon polariton, silicon photonic, waveguide, resonator, coupled mode, integrated optics

The potential of plasmonic devices for on-chip telecommunication applications and signal processing has generated increasing interest in recent years.[1] Propagating surface plasmon polaritons result from the collective oscillation of electrons at the interface of a metal and a dielectric in the presence of an electromagnetic field[2] and can support higher bandwidths than electrical signals carried by conventional metal wires. Compared with dielectric waveguides, plasmonic devices can concentrate light to smaller volumes and enhance light-matter interactions, but they suffer from metal-induced attenuation. Plasmonic waveguides with integrated gain media have been recently shown to exhibit enhanced propagation lengths by direct optical amplification at telecommunication[3,4] and other near-infrared[5,6] wavelengths; however, the impact of signal propagation loss on cm^2-scale integrated photonic chips can be minimized by using an architecture featuring short plasmonic waveguides coupled to longer dielectric waveguides.[7] This design approach significantly reduces overall chip-level waveguide losses relative to all-plasmonic networks, but the development of low-loss transitions between plasmonic and dielectric waveguides becomes critical.

The Si-on-insulator (SOI) photonics platform is emerging as the standard technology for optical systems on a chip. Researchers have recently demonstrated important optical components on SOI, including lasers[8] and photodetectors[9] operating near $\lambda = 1550$ nm. Thus, while the tremendous potential of surface-plasmon circuitry has been thoroughly explored,[10] integration with SOI can facilitate the realization of on-chip plasmonic devices that take advantage of components already developed for Si photonics. Furthermore, SOI waveguides can serve as low-loss interconnects for moving light between miniaturized plasmonic devices, minimizing overall on-chip losses.

Plasmonic waveguides have been previously demonstrated on SOI with lateral confinement achieved by patterning a metal film, and coupling efficiencies between 30 to 40% per transition were observed.[7,11,12] Metal slot waveguides have also been fabricated using Si wires as a mold for defining the waveguide shape,[13,14] and coupling efficiencies as high as 56% have been reported for devices supporting a single plasmonic mode. However, in all cases, these metal strip and slot waveguide designs have exhibited plasmon propagation lengths of less than 6 μm, limiting their utility in resonators and other interferometric devices. Very recently, Delacour et al. reported directional coupling to metal slot waveguides with predicted efficiencies comparable to those reported here; however, the exact efficiency is uncertain since the loss due to coupling and propagation were not measured independently.[15]

In contrast to patterned metal structures, dielectric-loaded surface plasmon polariton (DLSPP) waveguides confine surface plasmons laterally using a dielectric wire patterned on a flat metal film with typical plasmon propagation lengths on the order of 10 to 100 μm for wavelengths near $\lambda = 1550$ nm.[16,17] As optical components, DLSPP waveguides exhibit low enough propagation loss to be implemented in devices that require coherent propagation over many micrometers, such as ring resonators[18,19] and Bragg gratings.[20] Furthermore, for operation at telecommunication wavelengths, DLSPP devices can be fabricated using standard lithography processes, as opposed to V-groove plasmonic waveguides that can have similarly low losses but require advanced focused ion-beam fabrication.[21] To date, conventional meth-

* To whom correspondence should be addressed. E-mail: rbriggs@caltech.edu.
Received for review: 07/14/2010
Published on Web: 10/28/2010

DOI: 10.1021/nl1024529 | *Nano Lett.* **2010,** *10,* 4851–4857

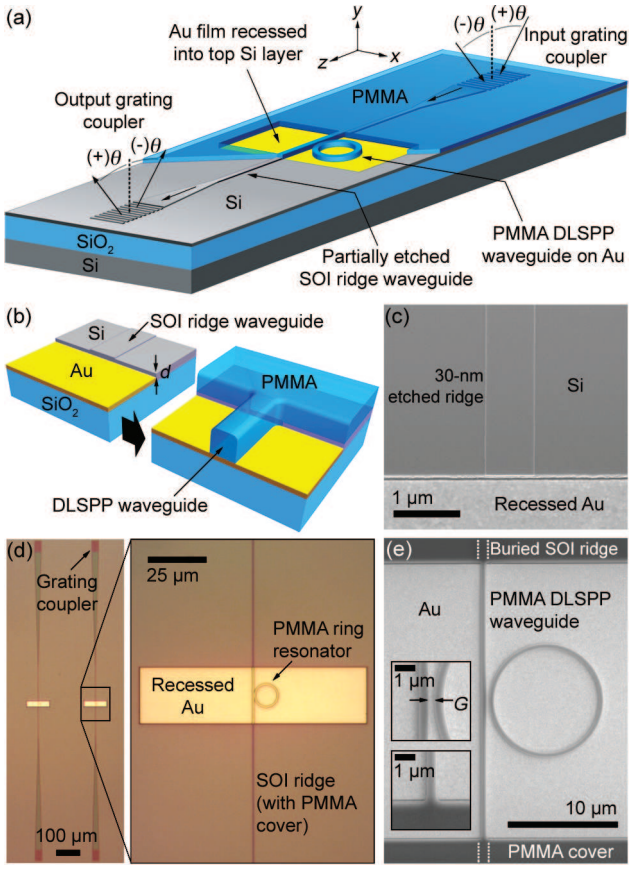

FIGURE 1. (a) Schematic of a SOI-waveguide-coupled DLSPP waveguide and ring resonator (not to scale). For clarity, the PMMA layer, which acts as both the dielectric load and a cover for the SOI waveguides, is shown partially removed from the output SOI waveguide. (b) Scale representation of the coupling region between end-coupled SOI and DLSPP waveguides before and after spinning and patterning of the PMMA cover layer. (c) Scanning electron micrograph of an etched Si ridge waveguide at the boundary of a recessed Au pad before coating with PMMA. (d) Optical micrographs of completed SOI-waveguide-coupled DLSPP devices. (e) Scanning electron micrograph of a DLSPP waveguide and ring resonator (coupling gap $G = 300$ nm) with buried SOI input/output waveguides.

ods for coupling light into DLSPP waveguides have employed external laser sources with off-chip optics (e.g., using the Kretschmann−Raether configuration[2]), which limits miniaturization at the system level. In a significant step toward integration with telecommunication technology, Gosciniak et al. recently demonstrated in- and out-coupling of light guided by DLSPP waveguides using single-mode optical fibers,[22] similar to schemes used to couple to weakly confined long-range surface plasmons.[23] However, there remains a need for integration of DLSPP waveguides on a photonics platform compatible with on-chip light sources and detectors.

In this letter, we present DLSPP waveguides and ring resonators composed of polymethylmethacrylate (PMMA) patterned on Au, which are integrated with low-loss SOI photonic circuits, as shown schematically in Figure 1a. We employ Si diffraction gratings to interface the SOI waveguides with an external laser source and detector; however, the devices reported here are compatible with SOI-integrated on-chip optical components and can be implemented in a low-temperature back-end wafer process. We first analyze the transmission through SOI-waveguide-coupled DLSPP waveguides of varying length and find that the DLSPP transmission decreases exponentially with a decay length of 51 ± 4 μm at $\lambda = 1550$ nm. This propagation length is reproducible at multiple grating coupling angles and wavelengths and is consistent with modal effective index calculations. Accounting for propagation loss, the coupling loss is found to be 1.0 ± 0.1 dB per transition between the SOI and DLSPP waveguides, which is in close agreement with full-field electromagnetic finite-difference time-domain (FDTD) simulations for the fabricated waveguide dimensions. Finally, we analyze the spectral response of 10 μm diameter DLSPP ring resonators and find an average intrinsic resonator quality factor of 180 ± 8 near $\lambda = 1524$ nm, where the resonator propagation length is limited by bending loss in the curved waveguide geometry.

SOI-waveguide-coupled DLSPP structures were fabricated on SOI wafer pieces with a lightly doped *p*-type ($\sim 10^{15}$ cm^{-3}) 220 nm Si device layer on a 2 μm buried oxide (BOX) layer. Arrays of 100 μm wide Au pads of varying length, L, were defined by electron-beam lithography using PMMA resist (MicroChem), where the polymer was used both as a mask for SF_6-based plasma etching of the top Si layer and as a lift-off layer for metallization. A 5 nm Ti sticking layer and an 80 nm Au layer were deposited into the etched regions by electron-beam evaporation. This Au film is thick enough to eliminate coupling of surface plasmons on the top surface into radiation modes in the underlying BOX layer.[24] In addition, since Ti absorbs more strongly than Au near $\lambda = 1550$ nm,[25] the sticking layer extinguishes unwanted surface plasmons on the bottom surface of the metal. The Si etch also consumed approximately 10 nm of the BOX layer, so that the top surface of the Au was recessed a depth $d = 145$ nm below the surrounding Si without additional etching of the SiO_2. We also fabricated samples using buffered hydrofluoric acid to remove approximately 150 nm of additional SiO_2 from the BOX layer prior to metallization, resulting in a Si−Au offset close to $d = 300$ nm.

Ridge waveguides were patterned on the Si surrounding the Au pads using negative-tone electron-beam resist (Micro Resist Technology ma-N 2403), and the exposed Si was partially etched to a depth of 30 nm with a C_4F_8/O_2 plasma etching process. The SOI waveguides were fabricated with a ridge width of 740 nm, as shown in Figure 1c, so that only the fundamental transverse-electric (TE) and transverse-magnetic (TM) modes are supported at the wavelengths of interest in this work. The waveguide dimensions were also chosen to fulfill the "magic-width" condition, which minimizes leakage loss from the TM mode.[26] For completed devices, we measured a SOI-waveguide propagation loss of 5.5 dB/cm near $\lambda = 1550$ nm for the TM mode and even lower loss for the TE mode (see Supporting Information). To

DOI: 10.1021/nl1024529 | *Nano Lett.* **2010,** *10,* 4851–4857

couple light into and out of the SOI waveguides, we defined symmetrical pairs of 30 μm wide, 50 μm long etched diffraction gratings with a 650 nm grating pitch, connected to the waveguides via 500 μm linear tapers, as shown in Figure 1d.

The surface of the samples were coated with 560 nm of PMMA, cured for 5 min at 180 °C, and patterned to define single-mode, 500 nm wide DLSPP waveguide straights on the Au pads with the straight DLSPP waveguides end-coupled to the SOI waveguides, as shown in Figure 1b. The 500 × 560 nm DLSPP waveguide cross section supports only the fundamental TM plasmonic mode (TM_{00}) with near-optimal modal confinement at $\lambda = 1550$ nm.[4,16,24] Devices were also fabricated with 10 μm diameter PMMA rings patterned alongside the straight DLSPP waveguides with a variable edge-to-edge separation gap, G. The PMMA was left on top of the SOI waveguides to serve as a dielectric cover. Micrographs of fabricated SOI and DLSPP waveguides are shown in Figure 1d,e. We used atomic force microscopy (AFM) to verify the dimensions of the waveguide structure and to determine the morphology of the PMMA structure at the SOI-DLSPP waveguide interface. The AFM measurements show that the cured PMMA layers conform to the surface of the recessed Au pads, resulting in a uniform layer thickness over the length of the DLSPP sections with a short vertical taper at the edges of the surrounding Si (see Supporting Information).

To determine the coupling efficiency between the SOI and DLSPP waveguides, we first characterized the surface plasmon propagation loss in the DLSPP structure. Assuming light propagates only in the fundamental mode of the polymer-on-Au waveguide, the theoretically predicted propagation loss is obtained from the imaginary part of the calculated modal effective index. In Figure 2a, we show the real part of the effective index for the modes supported by a DLSPP waveguide with the fabricated dimensions, calculated using the two-dimensional electromagnetic finite-element method (FEM). We assume an index of 1.49 for PMMA and an index of Au obtained by interpolating between the values measured by Johnson and Christy[27] (see Supporting Information). A TE-polarized dielectric mode is supported by the polymer wire for wavelengths shorter than $\lambda = 1300$ nm, but the structure supports only the fundamental TM_{00} plasmonic mode for the wavelength range of interest in this work.

Figure 2b shows the calculated DLSPP modal effective index and loss for wavelengths between $\lambda = 1500-1600$ nm. In addition to the nominal effective index and loss, we show the range of calculated values corresponding to the uncertainty in the Au index reported in ref 27. For $\lambda = 1500-1600$ nm, the modal effective index varies approximately linearly with a slope of $-0.27\,\mu m^{-1}$. The modal group index is calculated according to $n_g(\lambda) = n_{eff}(\lambda) - \lambda(\partial n_{eff}/\partial\lambda)$, which gives a value of approximately $n_g = 1.6$ for this wavelength range. While the uncertainty in the Au index does not lead to a significant spread in the calculated real effective index values, the modal loss is more sensitive, as shown in the lower panel of Figure 2b.

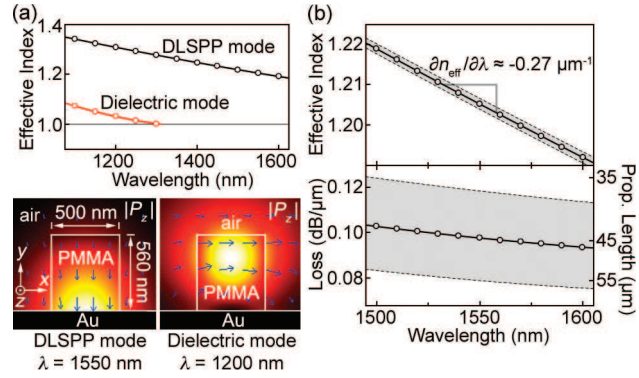

FIGURE 2. (a) Calculated modal dispersion of a DLSPP waveguide with the fabricated cross section. A TE-polarized dielectric mode is supported at wavelengths shorter than $\lambda \approx 1300$ nm, but only the DLSPP mode is supported at longer wavelengths. The density plots show the power in the propagation direction for each mode at the indicated wavelength, while the arrows represent the in-plane intensity and orientation of the electric field. (b) Dispersion of the DLSPP mode over the wavelength range of interest in this work, where the loss is obtained from the imaginary part of the modal effective index. The gray bands represent the range of predicted values resulting from the uncertainty in the refractive index of Au from ref 27.

We experimentally determined the plasmon propagation loss by measuring the transmission through devices with DLSPP sections of varying length on a sample with a Si−Au vertical offset of $d = 300$ nm. The transmission for each device was normalized to the average transmission through a set of SOI reference waveguides that were patterned on the same sample and tested under the same coupling conditions. To probe a particular device, light from a tunable diode laser with a tuning range of $\lambda = 1500-1575$ nm was focused onto the device's SOI input grating using a lensed fiber focuser (see Supporting Information). The optical axis of the focuser was positioned at an angle, θ, relative to the sample surface normal, as shown in Figure 1a. An identical focuser was positioned above the output grating at the same angle, and the overall device transmission was measured with either a calibrated power meter or, for spectrally resolved measurements, a high-speed photoreceiver. Within the wavelength range of the tunable laser, the Si gratings are designed to selectively couple light from free space to the forward-propagating fundamental TM mode of the SOI waveguides at $\theta \sim -30°$ and to the forward-propagating TE mode at $\theta \sim 30°$, taking advantage of the unique phase velocities of the two modes.[28]

To couple light into the TM-polarized DLSPP mode, we excited the TM SOI-waveguide mode near $\theta = -30°$ and adjusted a polarization controller on the input fiber to maximize transmission. The SOI gratings exhibit a limited bandwidth of approximately 25 nm; therefore, we made additional adjustments to the coupling angle to achieve maximum transmission at different wavelengths within the

DOI: 10.1021/nl1024529 | *Nano Lett.* **2010,** *10,* 4851–4857

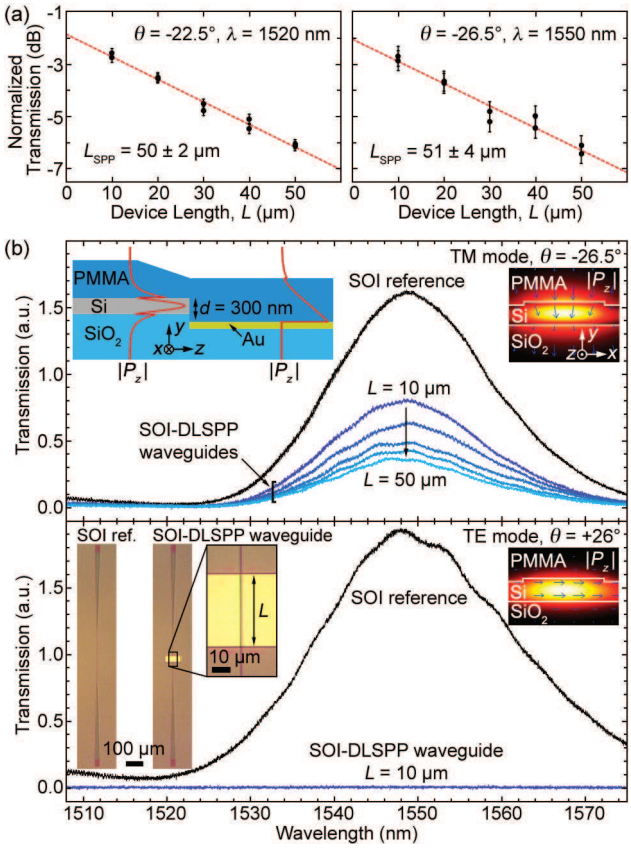

FIGURE 3. (a) TM-mode transmission through 10 devices with DLSPP sections of varying length, L, (two devices of each length) normalized to the average transmission through a set of three SOI reference devices. The error bars represent the uncertainty in the reference device measurements. The left panel shows the transmission at a grating coupling angle of $\theta = -22.5°$, corresponding to maximum transmission at $\lambda = 1520$ nm, while the right panel shows the transmission at $\lambda = 1550$ nm and a coupling angle of $\theta = -26.5°$. Both sets of measurements indicate a DLSPP propagation length of $L_{SPP} \approx 50\ \mu$m. By extrapolating to a device length of $L = 0$, the total coupling loss at $\lambda = 1550$ nm is 2.0 ± 0.2 dB, or 1.0 ± 0.1 dB per SOI-DLSPP transition. (b) Transmission spectra for coupling from the TM SOI-waveguide mode at a grating coupling angle of $\theta = -26.5°$ (top panel) and for coupling from the TE mode at $\theta = +26°$ (lower panel). The density plots show the calculated power distribution in the SOI-waveguide modes, where the arrows represent the in-plane electric field. A cross-section of the SOI-DLSPP structure is depicted in the inset in the top panel, while the inset in the lower panel shows optical micrographs of a SOI reference device and a SOI-DLSPP device with $L = 40\ \mu$m.

tuning range of the laser source. At a coupling angle of $\theta = -26.5°$, which corresponds to maximum transmission at $\lambda = 1550$ nm, we measured the transmission through 10 devices with DLSPP sections varying in length from $L = 10$ to 50 μm with two nominally identical devices of each length. The transmission is plotted as a function of device length in the right panel of Figure 3a, where the transmission values have been normalized to the average transmission through a set of three reference waveguides with no DLSPP section. For a laser power of 1 mW at the input fiber, we measured an average transmitted power of $24.6 \pm 2.2\ \mu$W at $\lambda = 1550$ nm for the reference devices, due predominantly to loss in the lensed fibers and grating couplers. By normalizing the DLSPP transmission by this value, we account for the expected fiber and grating-coupling loss in the SOI-DLSPP devices. In addition, the standard deviation of the average reference device transmission gives rise to the error bars for the normalized DLSPP-waveguide transmission values.

The transmission through the DLSPP waveguides decreases exponentially with increasing device length with a characteristic propagation length of $L_{SPP} = 51 \pm 4\ \mu$m. Extrapolating to a DLSPP waveguide length of $L = 0$, we find a total coupling loss of 2.0 ± 0.2 dB relative to the reference devices, or 1.0 ± 0.1 dB per SOI-DLSPP waveguide transition, where the uncertainty arises from the fit to the individual transmission values. We repeated the transmission measurements on the same devices at $\lambda = 1520$ nm for a grating coupling angle of $\theta = -22.5°$, as shown in the left panel of Figure 3a. We observe small differences in the relative transmission from one device to the next, but we find values for the propagation length and coupling loss that fall within the uncertainty of the values measured at $\lambda = 1550$ nm. This demonstrates that the measured coupling efficiency is reproducible despite inevitable variations in optical alignment between measurements. Furthermore, we note that the propagation length of $L_{SPP} \approx 50\ \mu$m falls within the range predicted by the FEM calculations. Finally, we performed near-field scanning optical microscopy (NSOM) measurements on the DLSPP waveguides and observed propagation lengths that are in agreement with the values determined from the waveguide transmission measurements (see Supporting Information).

We also performed transmission measurements on a sample with a Si−Au offset of $d = 300$ nm that was fabricated simultaneously with the previously characterized sample, except that the final PMMA coating step was excluded. Without a PMMA dielectric load, light can only couple from the input SOI waveguide to the output via radiation modes or surface plasmons at the Au−air interface. While we expect coupling to these other modes, we also expect the power to disperse radially from the end of the SOI input waveguide and therefore not couple significantly into the SOI output waveguide. Indeed, the lowest loss we measured relative to the SOI reference waveguides was 17.4 ± 0.4 dB for a device with a 10 μm long Au section, which is nearly six times greater loss than measured for DLSPP waveguides of the same length. Transmission via radiation and Au−air plasmon modes is likely even lower for DLSPP waveguide devices since coupling to those modes is impeded by the polymer wire. This finding supports the assumption that, for the DLSPP devices, light is transmitted to the SOI output waveguide almost exclusively through the single DLSPP mode.

In the top panel of Figure 3b, we show transmission spectra for one of the SOI reference waveguides as well as for DLSPP waveguides of each length, where light was

DOI: 10.1021/nl1024529 | Nano Lett. 2010, 10, 4851–4857

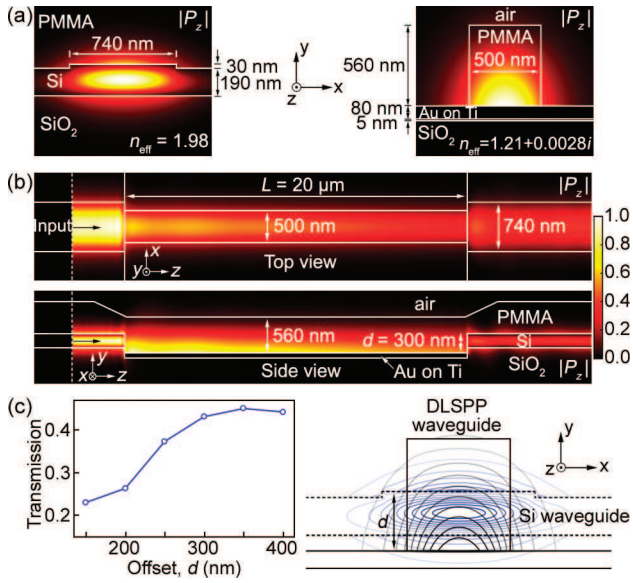

FIGURE 4. (a) Cross section and calculated power distribution in the propagation direction for the TM SOI-waveguide mode and the DLSPP mode at $\lambda = 1550$ nm. (b) Finite-difference time-domain (FDTD) simulations showing the power in the propagation direction at $\lambda = 1550$ nm through a 20 μm long DLSPP waveguide with input/output SOI waveguides. The vertical offset between the top Si and Au surfaces is $d = 300$ nm. The input power was launched in the TM SOI-waveguide mode at the indicated position. The top view corresponds to a plane cutting through the center of the Si waveguide perpendicular to the y-direction, 190 nm above the Au surface, and the side view corresponds to a plane bisecting the waveguide in the x-direction. (c) Total transmission through the 20 μm long DLSPP waveguide as a function of the Si−Au offset, d, calculated by FDTD. The contour plot shows the TM SOI-waveguide mode (blue) overlaid with the DLSPP mode (gray) for $d = 300$ nm.

coupled from the laser source into the TM SOI-waveguide mode. Other than the spectral lineshape characteristic of the SOI gratings, the DLSPP devices do not exhibit strong wavelength-dependent behavior over the wavelength range of interest. In the lower panel of Figure 3b, we show the spectral response of the same reference waveguide when light was coupled into the TE SOI-waveguide mode at a grating coupling angle $\theta = +26°$. Despite the higher transmission in the SOI waveguide for the TE configuration due to greater grating efficiency for that polarization, there is very little transmission through even the shortest DLSPP devices. Compared with the reference device TE-mode transmission of 30.1 μW at $\lambda = 1550$ nm, we measured less than 50 nW of transmitted power for the DLSPP devices with $L = 10$ μm. This polarization dependence indicates that there is negligible TE-to-TM mode conversion, and it further corroborates the assertion that light traverses the Au film only in the TM-polarized DLSPP mode and not through coupling to radiation modes.

To further verify the measured coupling efficiency, we modeled the three-dimensional waveguide structure using FDTD simulations, including input/output SOI waveguides and a 20 μm long DLSPP section, as shown in Figure 4b. At the waveguide transitions, we modeled the PMMA layer with a 2 μm long linear taper at the edge of the Si layer, in accord with AFM measurements of the fabricated topography (see Supporting Information). The calculated TM mode supported by the input SOI waveguide at $\lambda = 1550$ nm, plotted in Figure 4a, was used as the FDTD source, and we monitored the power transmitted through the output SOI waveguide 10 μm from the output transition. In Figure 4c, we show the total transmission calculated for different values of the Si−Au offset, d. The power profiles plotted in Figure 4b indicate that light is coupled predominately into the DLSPP mode, so it is reasonable to assume that light reaching the output monitor has traversed the Au region only through that mode. From FEM calculations at $\lambda = 1550$ nm using the nominal Au index,[27] the propagation loss for the DLSPP mode, plotted in Figure 4a, is 0.10 dB/μm. Given the total calculated transmission of 43.2% (3.65 dB loss) for $d = 300$ nm, we therefore estimate a loss of 2.0 dB due to mode attenuation for $L = 20$ μm. The modeled coupling loss is thus approximately 0.8 dB per SOI-DLSPP transition, slightly lower than the experimentally measured value of 1.0 ± 0.1 dB.

In addition to being potential building blocks for devices such as filters and modulators,[18,19,29] ring resonators provide a means for further characterizing the DLSPP waveguide mode. On a sample with a smaller Si−Au offset of $d = 145$ nm, we fabricated 10 μm diameter DLSPP rings with the same cross-section as the straight waveguides, where each ring is evanescently coupled to a straight 25 μm long DLSPP waveguide across a narrow coupling gap, as shown in Figure 1e. From the transmission spectra for the straight waveguides, we observe coupling to plasmonic whispering-gallery mode resonances; however, as the linewidth of the resonances is a significant fraction of the SOI grating bandwidth, we must account for the grating response. Upon identifying the spectral position of the ring resonator modes within the laser tuning range, we adjusted θ to maximize the grating efficiency near the central wavelength of each resonance. In the top panel of Figure 5, we show the raw transmission spectrum of a SOI-waveguide-coupled DLSPP reference waveguide (not coupled to any ring) for grating coupling angles of $\theta = -22.5$ and $-33°$. Because of angle-dependent interference within the PMMA/Si/SiO_2 dielectric stack, the grating efficiency is significantly higher for $|\theta| = 22.5°$ than for $|\theta| = 33°$, resulting in higher peak transmission at the smaller absolute coupling angle.[30] Also shown in the top panel of Figure 5 are the raw transmission spectra for three DLSPP waveguides, each coupled to a resonator across a different coupling gap, G. The lower panel of Figure 5 shows the corrected resonator transmission spectra, $T(\lambda)$, which are simply the raw transmission spectra divided by the reference device transmission at each wavelength. By normalizing the resonator transmission in this manner, we correct for both the SOI grating response and the propagation loss in the straight waveguides. Some error is introduced from variations in fabrication and optical alignment from one device to the next, as evidenced by the asymmetry in some of the

DOI: 10.1021/nl1024529 | *Nano Lett.* **2010,** *10,* 4851–4857

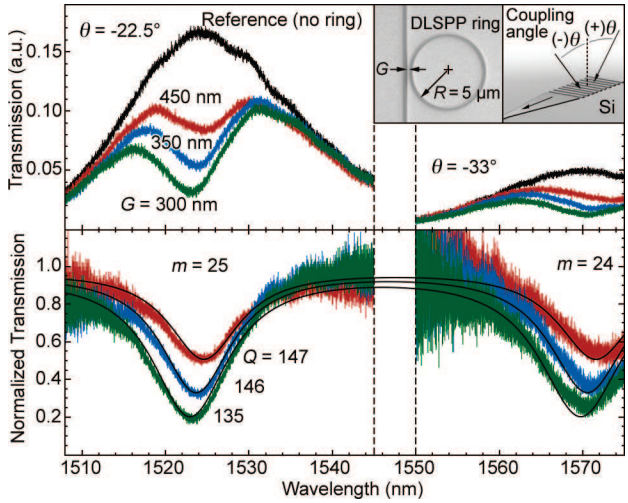

FIGURE 5. Transmission spectra of DLSPP waveguides evanescently coupled to ring resonators (radius $R = 5\ \mu$m) with a varying separation gap, G, collected at the indicated grating coupling angles, θ. The raw spectra in the top panel show the effect of coupling into whispering-gallery modes (azimuthal order m) as well as the SOI grating response. The normalized spectra in the lower panel were obtained by dividing by the transmission spectrum of a reference device with no ring in order to correct for the grating response. Fitted transmission curves for each ring are shown in black, along with the loaded Q factors of the $m = 25$ resonances.

corrected spectra; however, we are still able to compare the normalized spectra to a theoretical transmission model.

Examining the normalized resonator spectra, reduced transmission due to coupling into the rings is clearly visible near $\lambda = 1524$ and 1571 nm. The depths of the transmission minima increase with decreasing G, indicating that the resonators are undercoupled. Additionally, the resonance wavelength is blue shifted with decreasing G, consistent with the coupling-induced frequency shift theoretically predicted by Tsilipakos et al.[19] We fit the resonator spectra to the following functional form, adapted from the expression derived by Yariv for transmission through a waveguide coupled to a ring resonator[31]

$$T(\lambda) = \frac{a^2 + |t|^2 - 2a|t|\cos\left(\frac{2\pi n_{\mathrm{eff}}(\lambda)L_c}{\lambda} - \phi\right)}{1 + a^2|t|^2 - 2a|t|\cos\left(\frac{2\pi n_{\mathrm{eff}}(\lambda)L_c}{\lambda} - \phi\right)} \qquad (1)$$

where $L_c = 10\pi\ \mu$m is the ring circumference at the waveguide centerline and $n_{\mathrm{eff}}(\lambda)$ is the real part of the modal effective index, which we find to be negligibly different for the straight and curved waveguide geometries based on the resonator free-spectral range. The parameters a and $t = |t|\exp(i\phi)$ are related to the field attenuation due to propagation and coupling, respectively, where $a < |t|$ for an undercoupled resonator. The propagation loss in the ring, α_{prop}, is due in general to a combination of absorption in the Au and bending loss. The phase factor, ϕ, accounts for the additional phase accumulation due to coupling, which is responsible for the observed coupling-induced shift of the resonance wavelength. At the m^{th}-order resonance wavelength, λ_m, the phase accumulated in one round trip around the ring obeys the relation

$$\frac{2\pi n_{\mathrm{eff}}(\lambda_m)L_c}{\lambda_m} - \phi = 2\pi m, \quad m = 1, 2, 3\ldots \qquad (2)$$

Using the calculated $n_{\mathrm{eff}}(\lambda)$ plotted in Figure 2b, we fit eq 1 to the measured ring resonator transmission spectra with a, $|t|$, and ϕ taken as the only fitting parameters. The best-fit values of $|t|$ are 0.81, 0.86, and 0.90 for $G = 300$, 350, and 450 nm, respectively. The round-trip loss due to coupling, $l_{\mathrm{coup}} = -2\ln|t|$, therefore decreases with increasing coupling gap. The best-fit values of a range between 0.54 and 0.57 and, as expected, there is no clear trend with coupling gap. The corresponding cavity propagation length is $L_{\mathrm{prop}} = L_c/(-2\ln(a)) = 1/\alpha_{\mathrm{prop}}$, which has an average value of $27 \pm 1\ \mu$m for the three resonator devices. We neglect the wavelength dependence of L_{prop} since the loss due to Au absorption varies by less than 3% over the spectral range of our measurements. We can estimate the bending loss, α_{bend}, by assuming that the propagation length in the absence of bending effects is $L_{\mathrm{SPP}} \approx 50\ \mu$m, as previously measured for the straight waveguides, yielding $\alpha_{\mathrm{bend}} = \alpha_{\mathrm{prop}} - 1/L_{\mathrm{SPP}} \approx 0.074$ dB/μm, or 0.37 dB/rad. This bending loss agrees remarkably well with the value of 0.36 dB/rad determined by Holmgaard et al. from NSOM measurements for DLSPP ring resonators of the same diameter.[20] Finally, we recall that the DLSPP ring resonators were patterned on a sample with a Si−Au vertical offset of $d = 145$ nm, and we note that the total loss measured for the 25 μm long DLSPP reference device was 7.1 ± 0.1 dB relative to SOI reference waveguides patterned on the same sample. For $L_{\mathrm{SPP}} \approx 50\ \mu$m, this indicates a coupling loss of 2.5 dB per transition, in fair agreement with the value of 1.9 dB estimated from the FDTD simulations for $d = 150$ nm.

The quality factor for the m^{th}-order resonance is $Q = 2\pi c\tau_c/\lambda_m$, where c is the speed of light in vacuum and $\tau_c = n_g L_c/(cl)$ is the cavity lifetime, defined in terms of the modal group index, n_g, and the round-trip loss, l. The previously calculated value of $n_g = 1.6$ for the DLSPP mode near $\lambda = 1550$ nm can be corroborated by measuring the free-spectral range between adjacent resonances, $\Delta\lambda = \lambda_{m+1} - \lambda_m = \lambda_{m+1}\lambda_m/(n_g L_c)$. For the measured resonator spectra, we observe $\Delta\lambda \approx 47$ nm, which corresponds to $n_g = 1.62$. The good agreement with the value from two-dimensional FEM calculations indicates that the real part of the DLSPP modal index corresponding to a bend radius of $R = 5\ \mu$m is approximately equal the index of the straight-waveguide mode. The loaded Q factor of each $m = 25$ resonance is

DOI: 10.1021/nl1024529 | Nano Lett. 2010, 10, 4851–4857

indicated in Figure 5, which includes loss contributions from material absorption, coupling, and bending loss, so that $l = l_{coup} + \alpha_{prop}L_c$. Accounting only for absorption and bending loss, we define the intrinsic quality factor, Q_{int}, with $l = \alpha_{prop}L_c$. Since Q_{int} excludes loss due to coupling, it should be independent of G. Averaging over the measured devices, we find $Q_{int} = 180 \pm 8$ for the $m = 25$ resonance.

In summary, we have demonstrated efficient coupling of light in and out of polymer-on-Au DLSPP waveguides and ring resonators using low-loss SOI waveguides at telecommunication wavelengths. Accounting for propagation loss, we measured coupling loss of 1.0 ± 0.1 dB per SOI-DLSPP waveguide transition at $\lambda = 1550$ nm, corresponding to coupling efficiency of $79 \pm 2\%$. The devices demonstrated here show that DLSPP waveguides can be efficiently interfaced with optical systems fabricated on SOI to combine the advantages of plasmonics with the low propagation loss of Si photonic circuits. With the addition of SOI-integrated light sources and detectors, these plasmonic devices can be integrated into a compact, self-contained optical system on a chip.

Acknowledgment. This work was supported by the Air Force Office of Scientific Research under MURI Award FA9550-06-1-0470 and Grant FA9550-09-1-0673. The authors gratefully acknowledge critical support and infrastructure provided by the Kavli Nanoscience Institute at Caltech. R.M.B. appreciatively acknowledges support from the National Defense Science and Engineering Graduate Fellowship and also thanks K. Aydin, D. Chi, and A. Yariv for helpful discussions.

Supporting Information Available. Experimental details on grating coupling and SOI waveguide characterization, additional information on electromagnetic calculations, AFM measurements of waveguide dimensions, and NSOM measurements of the surface plasmon propagation length. This material is available free of charge via the Internet at http://pubs.acs.org.

REFERENCES AND NOTES

(1) Zia, R.; Schuller, J. A.; Chandran, A.; Brongersma, M. L. *Mater. Today* **2006**, *9*, 20–27.
(2) Raether, H. *Surface Plasmons on Smooth and Rough Surfaces and on Gratings*; Springer: New York, 1988.
(3) Ambati, M.; Nam, S. H.; Ulin-Avila, E.; Genov, D. A.; Bartal, G.; Zhang, X. *Nano Lett.* **2008**, *8*, 3998–4001.
(4) Grandidier, J.; des Francs, G. C.; Massenot, S.; Bouhelier, A.; Markey, L.; Bouhelier, A.; Weeber, J. C.; Finot, C.; Dereux, A. *Nano Lett.* **2009**, *9*, 2935–2939.
(5) De Leon, I.; Berini, P. *Nat. Photonics* **2010**, *4*, 382–387.
(6) Gather, M. C.; Meerholz, K.; Danz, N.; Leosson, K. *Nat. Photonics* **2010**, *4*, 457–461.
(7) Hochberg, M.; Baehr-Jones, T.; Walker, C.; Scherer, A. *Opt. Express* **2004**, *12*, 5481–5486.
(8) Fang, A. W.; Park, H.; Cohen, O.; Jones, R.; Paniccia, M. J.; Bowers, J. E. *Opt. Express* **2006**, *14*, 9203–9210.
(9) Ahn, D.; Hong, C.-Y.; Liu, J.; Giziewcz, W.; Beals, M.; Kimerling, L. C.; Michel, J.; Chen, J.; Kärtner, F. X. *Opt. Express* **2007**, *15*, 3916–3921.
(10) Ebbesen, T.; Genet, C.; Bozhevolnyi, S. I. *Phys. Today* **2008**, *61*, 44–50.
(11) Tian, J.; Yu, S.; Yan, W.; Qiu, M. *Appl. Phys. Lett.* **2009**, *95*, No. 013504.
(12) Han, Z.; Elezzabi, A. Y.; Van, V. *Opt. Lett.* **2010**, *35*, 502–504.
(13) Chen, L.; Shakya, J.; Lipson, M. *Opt. Lett.* **2006**, *31*, 2133–2135.
(14) Yang, R.; Wahsheh, R. A.; Lu, Z.; Abushagur, M. A. G. *Opt. Lett.* **2010**, *35*, 649–651.
(15) Delacour, C.; Blaize, S.; Grosse, P.; Fedeli, J. M.; Bruyant, A.; Salas-Montiel, R.; Lerondel, G.; Chelnoko, A. *Nano Lett.* **2010**, *10*, 2922–2926.
(16) Holmgaard, T.; Bozhevolnyi, S. I. *Phys. Rev. B* **2007**, *75*, 245405.
(17) Holmgaard, T.; Bozhevolnyi, S. I.; Markey, L.; Dereux, A. *Appl. Phys. Lett.* **2008**, *92*, No. 011124.
(18) Holmgaard, T.; Chen, Z.; Bozhevolnyi, S. I.; Markey, L.; Dereux, A. *Opt. Express* **2009**, *17*, 2968–2975.
(19) Tsilipakos, O.; Yioultsis, T. V.; Kriezis, E. E. *J. Appl. Phys.* **2009**, *106*, No. 093109.
(20) Holmgaard, T.; Chen, Z.; Bozhevolnyi, S. I.; Markey, L.; Dereux, A.; Krasavin, A. V.; Zayats, A. V. *Appl. Phys. Lett.* **2009**, *94*, No. 051111.
(21) Bozhevolnyi, S. I.; Volkov, V. S.; Devaux, E.; Laluet, J.-Y.; Ebbesen, T. W. *Nature* **2006**, *440*, 508–511.
(22) Gosciniak, J.; Volkov, V. S.; Bozhevolnyi, S. I.; Markey, L.; Massenot, S.; Dereux, A. *Opt. Express* **2010**, *18*, 5314–5319.
(23) Berini, P.; Charbonneau, R.; Lahoud, N.; Mattiussi, G. *J. Appl. Phys.* **2005**, *98*, No. 043109.
(24) Grandidier, J.; Massenot, S.; des Francs, G. C.; Bouhelier, A.; Weeber, J. C.; Markey, L.; Dereux, A.; Renger, J.; Gonzalez, M. U.; Quidant, R. *Phys. Rev. B* **2008**, *78*, 245419.
(25) *Handbook of Optical Constants of Solids*; Palik, E. D., Ed.; Academic Press: New York, 1985.
(26) Webster, M. A.; Pafchek, R. M.; Mitchell, A.; Koch, T. L. *IEEE Photonics Technol. Lett.* **2007**, *19*, 426–431.
(27) Johnson, P. B.; Christy, R. W. *Phys. Rev. B* **1972**, *6*, 4370–4379.
(28) Briggs, R. M.; Shearn, M.; Scherer, A.; Atwater, H. A. *Appl. Phys. Lett.* **2009**, *94*, No. 021106.
(29) Gosciniak, J.; Bozhevolnyi, S. I.; Anderson, T. B.; Volkov, V. S.; Kjelstrup-Hansen, J.; Markey, L.; Dereux, A. *Opt. Express* **2010**, *18*, 1207–1216.
(30) Masturzo, S. A.; Yarrison-Rice, J. M.; Jackson, H. E.; Boyd, J. T. *IEEE Trans. Nanotechnol.* **2007**, *6*, 622–626.
(31) Yariv, A. *Electron. Lett.* **2000**, *36*, 321–322.

DOI: 10.1021/nl1024529 | *Nano Lett.* **2010,** *10,* 4851–4857